Renewable Energy 227 (2024) 120503

Contents lists available at ScienceDirect

Renewable Energy

journal homepage: www.elsevier.com/locate/renene

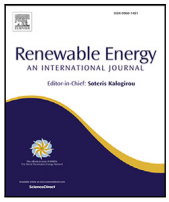

4P operational harmonic and blade vibration in wind turbines: A real case study of an active yaw system and a concrete tower

Antonio Torres [a,b,c,*], Javier Gil [b], Aitor Plaza [a], Jokin Aginaga [a,c]

[a] Public University of Navarre (UPNA), Campus de Arrosadía, Pamplona, 31006, Navarra, Spain
[b] Nordex Energy Spain S.A, Avenida Ciudad de la Innovación 3, Sarriguren, 31621, Navarra, Spain
[c] ISC-Institute of Smart Cities (UPNA), Campus de Arrosadía, Pamplona, 31006, Navarra, Spain

ARTICLE INFO

Keywords:
Wind turbine
Blade vibration
Operational resonance
Backward whirling mode
Active yaw system
Concrete tower

ABSTRACT

This study aims to comprehensively investigate the impact of mechanical loads on the performance and lifetime of wind turbines, with particular emphasis on blade vibration at the 4P operational harmonic. Experiments and advanced aeroelastic simulations are combined to assess how active yaw systems and concrete towers affect this specific vibration. Contrary to previous assumptions, field tests have shown that there is a resonance phenomenon in the blade. Specifically, the first edgewise mode of the blade resonates at the 4P frequency, which did not happen in the aeroelastic simulations. Remarkably, thorough aeroelastic simulations show that this resonance is triggered by the excitation of the Edgewise Backward Whirling mode of the rotor, which occurs at the 3P operating harmonic. This study highlights the need for accurate and precise modelling using aeroelastic simulations to reproduce the resonance phenomenon and analyse the contributing factors. A major breakthrough is the discovery that stiffening the active yaw system significantly reduces the 3P hub fixed motions, resulting in reduced blade vibration at the 4P frequency. Furthermore, the simulations show the sensitivity of the 4P vibration to different wind characteristics, providing valuable insights for the design of wind turbines in different environmental conditions.

1. Introduction

Blade vibration due to the operational harmonics in horizontal axis wind turbines is a problem that is usually analysed at the design stage of a blade. Wind turbine (WT) manuals [1–3] give a general explanation of the theoretical details of this phenomenon. In practice, it is common to have vibrations that need to be analysed specifically for a particular WT and wind farm [4–6].

The risk of unexpected vibrations has increased in recent years for a number of reasons. In response to the need to minimise the cost of energy (CoE) of wind farms, innovative solutions have been developed. These include the use of larger rotors [7] and the construction of more slender towers [8]. Consequently, these advances lead to lower natural frequencies for these critical components. As a result, the frequencies of the larger turbine components are more likely to overlap with the operational harmonics.

The design of the wind farm layout is also important. It can include positions with very high turbulence intensity, which can generate high periodic disturbances. These disturbances are aligned with the blade passing frequency (1P) and its harmonics (3P, 6P, 9P...) in the fixed reference frame. The disturbances at 3P are mainly induced by wind turbulence, wind shear, wind direction, flow inclination angle and tower shadow [9–11]. These disturbances have the potential to significantly increase the excitation level of resonances at certain frequencies.

This research analyses a real case of unexpected blade vibration in a 4.8 MW wind turbine. The turbine analysed has an active yaw system and a prestressed concrete tower, which is known for its high stiffness compared to conventional steel towers, resulting in reduced vibration at higher tower heights [12]. The torsional dynamics of the tower directly influence the dynamic behaviour of the yaw system as they are in series on the same axis.

During the load validation process [13,14] performed on a prototype WT manufactured by Nordex, an unexpected vibration was detected in the blades. This vibration did not appear in the simulations previous to the validation process. The vibration is attributed to the first eigenfrequency of the blade in the edgewise direction and poses a particular challenge due to the specific configuration of the turbine. This paper presents a comprehensive analysis of this complex vibration phenomenon, with the aim of unravelling its underlying causes, modifying the aeroelastic model to reproduce it and exploring its implications.

* Corresponding author at: Public University of Navarre (UPNA), Campus de Arrosadía, Pamplona, 31006, Navarra, Spain.
E-mail address: torres.39760@e.unavarra.es (A. Torres).

https://doi.org/10.1016/j.renene.2024.120503
Received 26 November 2023; Received in revised form 12 April 2024; Accepted 14 April 2024
Available online 16 April 2024

There are several studies that have investigated resonant vibrations in wind turbines. Tibaldi et al. [15] concluded that operating close to resonance can lead to significant vibration levels, even with small differences in turbine characteristics, with particular focus on the structural pitch. Sullivan [16] investigated resonance in two-bladed wind turbines and showed that vibrations are noticeable when resonating with external excitations up to 5P in the blade edgewise mode. In addition, Fleming et al. [17] investigated vibrations in a three-bladed turbine, specifically addressing resonance at the high speed shaft and nacelle acceleration. The importance of accurately modelling the stiffness characteristics of the yaw structure was also highlighted in Maalawi [18], although not in the context of an active yaw system without a braking system. In this case, it is very relevant to reproduce the dynamic behaviour of the yaw system during turbine vibrations, as the yaw system is not fully restricted by the brakes. This issue has not yet been investigated in detail, as this yaw system configuration is relatively new.

To accurately reproduce mechanical resonance in wind turbines, the correct use of aeroelastic simulation tools is paramount, as analysed by Hach et al. [19], Holierhoek [20], Gözcü and Verelst [21] and Sayed et al. [22]. These tools allow accurate simulation of the complex interactions between aerodynamic, inertial and gravitational forces required to capture the intricate dynamics of the system. In addition, Filsoof and Zhang [23], Filsoof et al. [24] and Wanke et al. [25] have also investigated the vibration phenomenon of the Edgewise Backward Whirling (EBW) mode, providing additional insight into this particular aspect of wind turbine dynamics.

The aim of this investigation is to understand the vibration phenomenon observed in the field and to study the influence of the wind conditions and the flexibility of the active yaw system. In this case, the focus is specifically on the resonance of the EBW mode with the 3P in the fixed frame of reference, which is the one that has been experimentally found to be amplified. It also highlights the importance of accurately modelling the active yaw system and the prestressed concrete tower to gain insight into their specific contributions to the observed wind turbine vibrations.

The paper is structured as follows: It begins with the presentation of unexpected vibration results from a field study of a real WT. It then proceeds with an analysis of the vibration patterns and resonant frequencies of the investigated turbine configuration, together with insights into the interaction between the EBW mode and the 3P operational harmonic. The following section focuses on the modelling and simulation required to reproduce the unexpected vibration. A sensitivity analysis section is also included to investigate the effect of yaw stiffness on the observed vibration and to explore the influence of wind conditions. Finally, a summary section outlines the main findings of the research.

2. Field observation

During the load validation process of a Nordex WT prototype, anomalous behaviour of the blade root edgewise bending moment (from now on, M_x) was observed. This WT has a rated power of 4.8 MW, a rotor diameter of 155 m and a concrete tower of 120 m.

The edgewise bending moment of the blade is mainly due to gravity, and this gravitational cycle is repeated with each revolution of the rotor (1P). When the observer is in the rotating reference system of the blade, the vertical gravitational load is seen as sinusoidal. In this case, a 4P frequency load appears superimposed on the 1P frequency gravitational load. This effect significantly increases fatigue and extreme loads and can affect the performance and lifetime of the wind turbine. Fig. 1 shows an example of a time series of blade edgewise loads measured with strain gauges at the blade roots, showing the common vibration at 1P (an example marked in blue) and above it a clear vibration of four cycles (marked in red).

Fig. 2 shows the same *Blade 1* M_x signal from Fig. 1 in the frequency domain, and it can be seen that the highest power content is at the frequency 1P, followed by the frequency close to 4P.

To better understand the observed 4P vibration, an order analysis is performed based on the waterfall plot. Order analysis is used to quantify vibration in rotating machines whose speed changes with time. Fig. 3 shows the measured blade edgewise load in the frequency domain with the rotor frequency (multiples of P) on the x-axis and the rotor speed on the y-axis. The load is shown in the rotating reference frame and the power content of the blade edgewise load is shown in decibels on the colour scale.

It can be seen that 1P is the order with the highest vibration energy over the whole speed range of the rotor and also that its harmonics have low energy. Of particular interest is the hyperbolic curve showing the first eigenfrequency of the blade edgewise and its intersections with 5P at variable speed and, in particular, with 4P close to the rotor rated speed (Ω_{rated}). The edgewise vibration of the 4P blade close to Ω_{rated} is the most relevant resonance as it is higher than expected and it is therefore the main topic of this article.

3. Understanding 4P blade edgewise vibration

This section explains the blade edgewise vibration as a part of the rotor vibration at the 4P frequency, including an examination of the Campbell diagram.

In the design phase of a wind turbine blade, it is essential to avoid the occurrence of a resonance condition, in which the natural frequency of the blade is equal to the rotational frequency or to a harmonic with significant energy. The analysis of this phenomenon is usually carried out using a Campbell diagram, which shows, among others, the natural frequencies of the blades as a function of the rotor speed, including the rotational frequency and its harmonics [26,27]. Any intersection of the lines with a blade natural frequency over the operating speed range of the turbine indicates a *potential* resonance. These cases need to be analysed in detail to know the criticality for the structural integrity of the blade.

The Campbell diagram can be displayed showing the modes of the rotor with respect to the rotating reference frame or with respect to the fixed nacelle reference frame. When they are measured in the rotating reference frame, the multi-blade coordinate transformation [28,29] is used to generate the rotor modes with respect to the fixed reference frame.

Before starting to analyse the Campbell diagrams, it is convenient to give an introduction to the so-called rotor modes. Thirstrup Petersen et al. [30] has provided an explanation of how local edgewise vibrations in wind turbines can be coupled to the substructure of the whole rotor, leading to the occurrence of global Edgewise Forward Whirling (EFW) and Backward Whirling modes. These modes generate a force at the hub centre, resulting in either co-rotating or counter-rotating rotor CoG (centre of gravity) rotation relative to shaft rotation.

Fig. 4 illustrates the three rotor modes that are generated from the edgewise modes of each blade:

- Rotor 1st edgewise mode A: This is a synchronous mode as the three blades reach their maximum and minimum deflections simultaneously. It has a significant contribution from the drive train first torsional mode, resulting in an increase in the global mode frequency due to the stiffness of the low-speed shaft. This frequency does not correspond to the vibration observed in the field measurements described in Section 2. The vibrations associated with this mode can be reduced by using the torque control of the converter [31–33], due to the high contribution of the drive train mode.

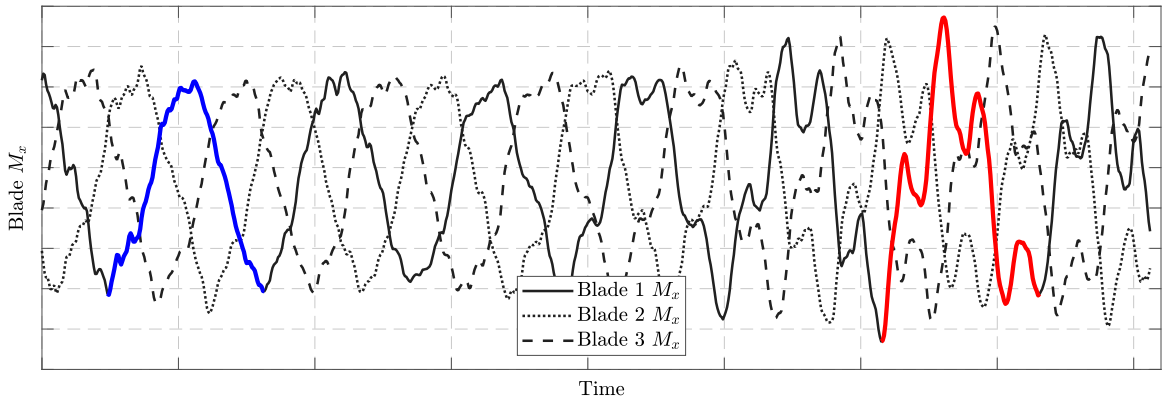

Fig. 1. Time series of measured edgewise loads on the three blade roots. A common 1P cycle is shown in blue and a clear vibration of four cycles is shown in red. Note: The axes are not labelled with absolute values and are provided for illustrative purposes only in order to protect the confidential information of the Nordex company.

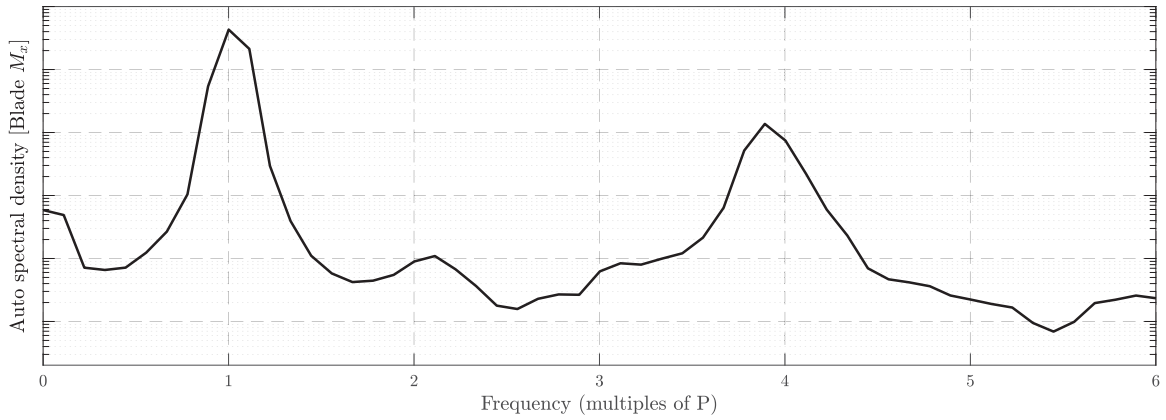

Fig. 2. Auto spectral density of the blade edgewise load in the frequency domain shown as a function of rotor speed.

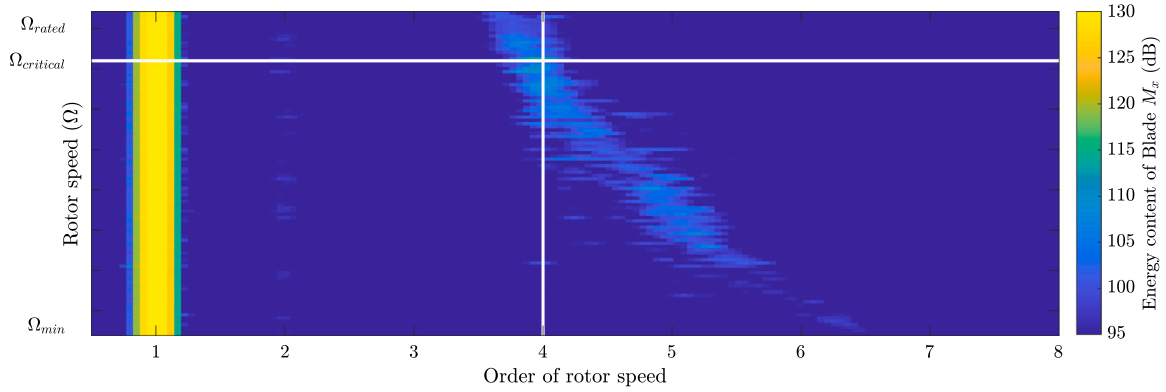

Fig. 3. Waterfall diagram of blade M_x order analysis. The white lines indicate the critical rotor speed ($\Omega_{critical}$) at which the 4P crosses the blade natural frequency.

- Rotor 1st edgewise mode B: This is an asynchronous mode as the three blades do not reach their maximum and minimum deflections simultaneously. The main contributions are the first edgewise modes of the three blades. In this case, the Campbell diagram has been calculated with blade 1 in the vertical and upward position. In this rotor mode B, the contribution of the first edgewise mode of blade 1 is more than three times the individual contributions of blades 2 and 3.
- Rotor 1st edgewise mode C: This is an asynchronous mode similar to mode B except that the individual contributions of the first edgewise modes of blades 2 and 3 are more than three times the contribution of blade 1.

Firstly, the Campbell diagram in Fig. 5 is shown in relation to the axes that move with the rotor, as these are the axes of the strain gauges that measured the 4P vibration. Secondly, the Campbell diagram in Fig. 6 is analysed in the fixed nacelle axes to see the operating frequencies that can excite the rotor modes from the fixed part of the turbine.

The diagram in Fig. 5 shows the existence of three rotor modes with a significant contribution from the first blade edgewise mode. There are two rotor edgewise modes (B and C) which cross the 4P operational frequency near Ω_{rated} and whose frequencies correspond to the observations seen in the field measurements described in Figs. 1 and 3.

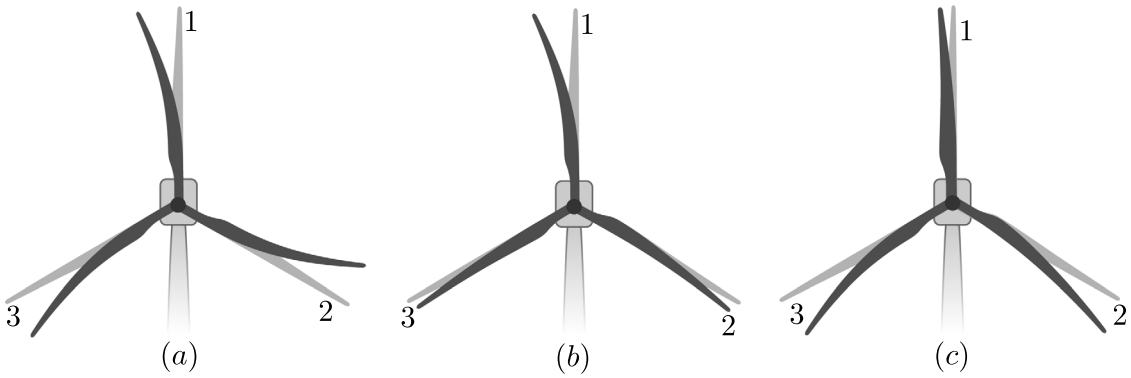

Fig. 4. The first edgewise mode shapes of the rotor. (a) Rotor 1st edgewise mode A (collective), (b) Rotor 1st edgewise mode B (anti-phase I) and (c) Rotor 1st edgewise mode C (anti-phase II).

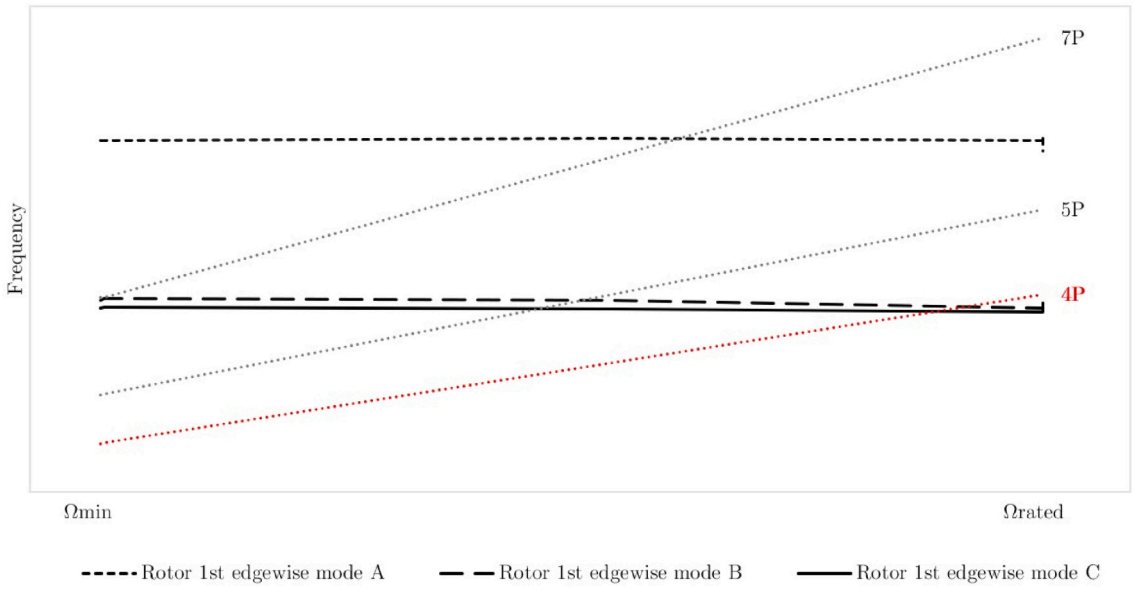

Fig. 5. Campbell diagram in the rotating frame of reference. The 4P operational frequency is highlighted in red.

Fig. 6 shows the Campbell diagram of the rotor under consideration in the fixed frame of reference. Only the 3P and 6P operational harmonics are shown as these are the most relevant for fixed frame turbine loads, with 3P highlighted in red as the most important.

There are three rotor modes with relevant participation of the first blade edgewise mode:

- Rotor 1st edgewise collective: This mode is the same as "Rotor 1st edgewise mode A" as it is not affected by the multi-blade coordinate transformation.
- Rotor 1st EFW: This is the asynchronous mode whose frequency increases by 1P as the rotor speed varies.
- Rotor 1st EBW: This is the asynchronous mode whose frequency decreases by 1P as the rotor speed varies. There is a potential resonance with 3P near Ω_{rated}, which seems to be important due to the usual large magnitude of 3P loads in the fixed reference frame.

With the multi-blade transformation, the EFW and EBW modes appear and it is possible to see which is being excited. In this case the EBW mode is excited by the 3P operational harmonic. It is interesting to note that the EBW mode is the one in which the rotor CoG rotates in the opposite direction to the rotor rotation. This has the effect of reducing the natural frequency as the speed increases [23].

Another variation of the Campbell diagram is shown in Fig. 7, in which the wind speed at hub height is plotted on the abscissa. In this way, resonances can be seen over the entire wind speed range, making it possible to distinguish between resonances at the same rotor speed but at different wind speeds.

It can be seen that the rotor first EBW mode is very close to 3P when the wind speed is higher than the rated wind speed (V_{rated}) and it is known that the 3P loads in the fixed part of the turbine increase with increasing wind speed and reach their maximum value near the cut-off wind speed [34]. This, together with the considerable number of hours that the turbines operate at Ω_{rated}, indicates that the 3P loads in the fixed part can have a significant effect on this mode of vibration. It is noticeable that above V_{rated} the pitch controller starts and the blade edgewise loads do not exactly match with the rotor inplane loads.

4. Modelling and simulation

The Campbell diagram illustrates the potential resonance points between the coupled turbine modes and the operational harmonics. In order to determine whether these resonances present any problems, the matter must be analysed using aeroelastic simulations, which require accurate modelling to reproduce the observed resonance phenomenon.

As mentioned above, the turbine model used in this study includes a concrete tower and an active yaw system. It should be noted that

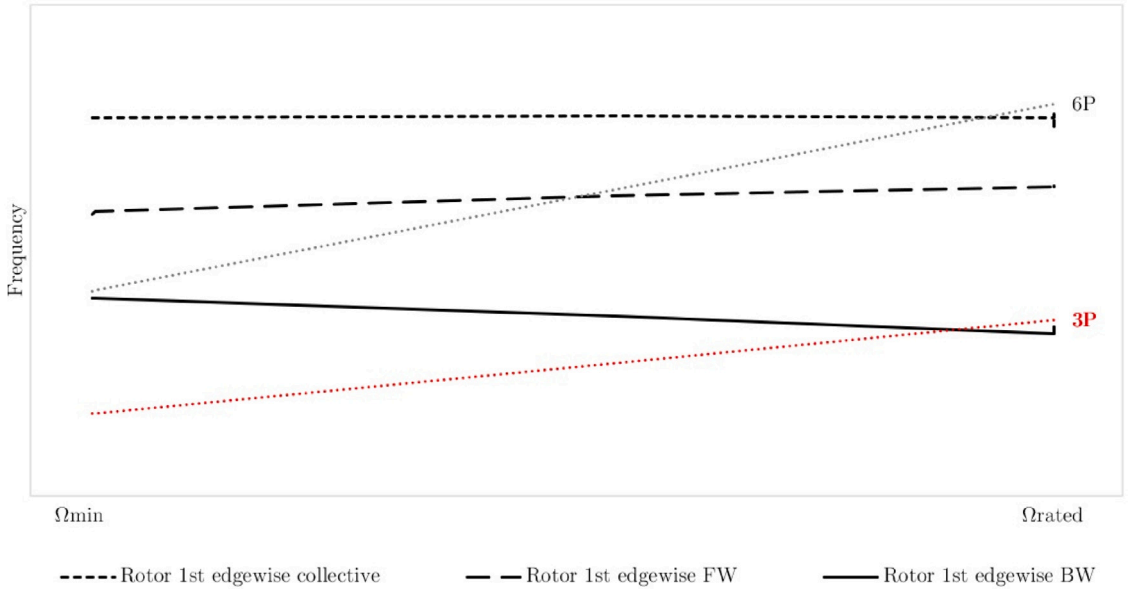

Fig. 6. Campbell diagram in the nacelle fixed frame of reference. The 3P operational frequency is highlighted in red.

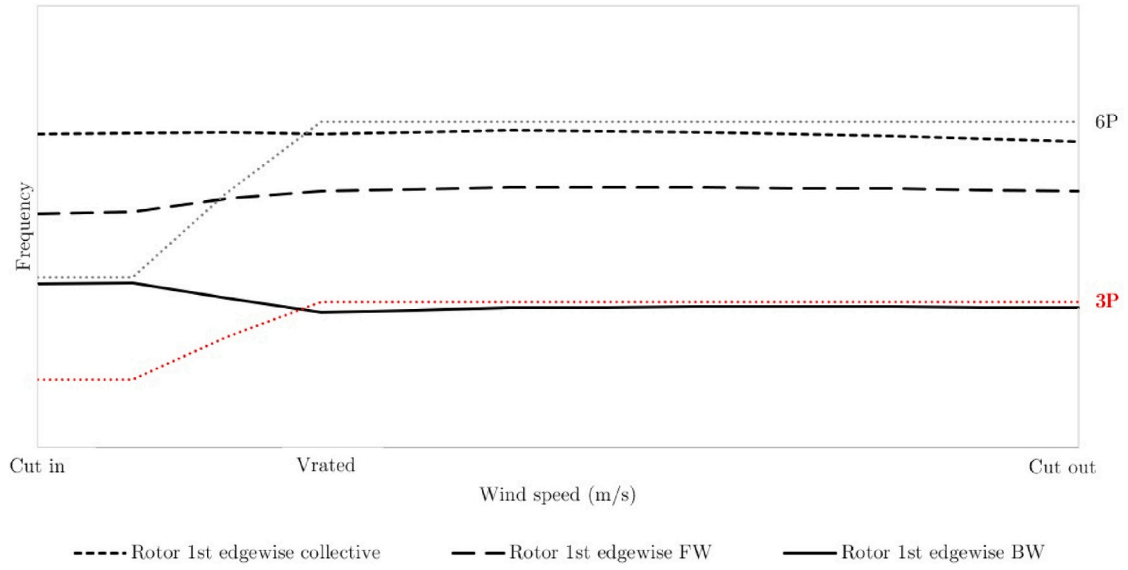

Fig. 7. Modified Campbell diagram (shown as a function of wind speed, from cut-in to cut-out). The 3P operational frequency is highlighted in red.

it is particularly important to accurately model these components as they are interrelated and dynamically affect each other, meaning that changes in one component can affect the behaviour of the other. The inclusion of an additional Degree of Freedom (DoF) representing the flexible yaw system is the main new feature of the model with respect to previous models that did not predict the unexpected experimental resonance. This new DoF improves the representation of the mechanics of the yaw system, which is necessary to reproduce the resonance phenomenon under investigation.

A new output variable is also introduced in this section to quantify and analyse the EBW mode vibration by filtering the moment M_x at the EBW mode frequency. The following subsections describe the nature of this variable and its validation.

4.1. Aeroelastic code and modelling

The aeroelastic design software used in this investigation is Bladed [35–37] and the specific modelling requirements essential to replicate the observed vibrations in the field are detailed below. It is crucial to ensure that the simulation model includes all relevant stiffness parameters and DoFs.

The tower is modelled by specifying its properties at a number of locations, starting at the base and progressing to the top. At each location the properties of the tower such as geometry, mass, bending stiffness, torsional stiffness and shear flexibility are defined. The foundation component is also included and its connection to the ground is represented by fore-aft and side-to-side bending DoFs. The transmission of the drive train takes into account the bending and torsional flexibility of the low-speed shaft. The nodding flexibility of the main frame is also included. The blade model includes geometric, mass and stiffness properties as well as its aerodynamic properties. Both bending and torsional flexibility are considered. The blade model is subdivided into many rigidly coupled finite element bodies to more rigorously model large blade deflections. The outer parts of the blade can undergo rigid body rotation as a function of the deflection and rotation of the inner parts, as well as incorporating linear deflections within the part.

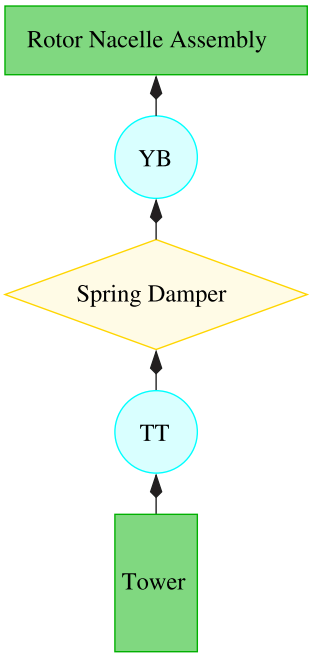

Fig. 8. Simplified yaw system model scheme.

The structural formulation is based on linear finite element bodies, supplemented by non-linear geometric stiffness models that take into account the effect of structural deflections on the dynamics. For flexible structures, the Craig–Bampton modal reduction method [38,39] is applied to calculate the component uncoupled modes of the tower and the blades. The modes of different bodies are coupled by the equations of motion so that the actual eigenfrequencies of the coupled system differ from the uncoupled mode frequencies. The aerodynamic calculations are performed using the momentum theory of Glauert [40], the dynamic wake model of Øye [41], the skew wake correction model Glauert [42,43] and the in-compressible Beddoes–Leishman dynamic stall model [44].

The wind turbine controller uses several strategies to manage the variable speed turbine with a double-fed induction generator [45,46]. During very low wind conditions, a PID controller is used to maintain the rotor speed at the minimum operating value. During periods of low wind, the reactive torque of the generator is modulated to optimise energy capture. In moderate wind conditions, a torque demand adjustment procedure is used to maintain the rotor speed at the rated value. In high wind conditions, pitch control [47] is used to regulate the rotor speed by adjusting the blade pitch angle with a feedback controller. In addition, individual pitch control is used to reduce the loads on the turbine [48].

The active yaw system and the concrete tower are critical for the dynamic performance of the WT. Thus, as the main novelty of the aeroelastic model, the yaw system is modelled as flexible, with the nacelle passively adjusting its angle in response to aerodynamic forces. A spring damper element is used to define the damping and stiffness of the angular connection between the tower and the nacelle. In Section 5.1, some stiffness values of the flexible yaw are analysed.

A schematic representation of the simplified yaw system used in the aeroelastic model is shown in Fig. 8, where the green boxes represent the components, the blue circles represent the tower top (TT) and yaw bearing (YB) output nodes, and the orange diamond is the new proposed spring damper element.

To analyse the vibration of the blade at its first natural frequency in the edgewise direction, a new output variable is created. This is obtained by filtering the M_x signal with a bandpass filter centred on the first edgewise natural frequency. The amplitude of the filtered signal is called BMX1EF. Fig. 9 shows an example of the M_x filtered signal (represented by black dots) corresponding to the M_x load, together with the amplitude of the filtered signal called BMX1EF (represented by red lines). This metric is used to quantify the vibration level of M_x at the first edgewise natural frequency of the blade. As can be seen from the graph, the BMX1EF indicator rises when the resonance of the edgewise BW mode is excited.

4.2. Validation of the proposed aeroelastic model and comparison with the conventional rigid yaw model

To validate the proposed aeroelastic model, the normal power production load cases (DLC1.2) of Class B turbulence intensity, as specified in the IEC61400-1 ed4 standard [49], are being used. As aforementioned, in order to reproduce the observed vibration, a modification of the stiffness of the yaw system was introduced in the wind turbine model. The results obtained are analysed in this section. The proposed modification of the yaw system model and its sensitivity to the BMX1EF vibration are shown in Fig. 10. The newly introduced flexible yaw modelling is contrasted with the conventional version of rigid yaw modelling in terms of normalised M_x in inlet-a and normalised BMX1EF in inlet-b.

It is important to highlight the effect of including the compliance of the yaw spring in the modelling process, as opposed to assuming a rigid yaw system. It is observed in inlet-b of Fig. 10 that when the stiffness of the yaw spring was included in the model, the simulation of the BMX1EF vibration showed higher levels that were representative of those measured experimentally.

By incorporating the compliance of the yaw spring, the new model is able to reproduce the unexpected amplification of the edgewise mode observed experimentally in the field, as shown in inlet-a of Fig. 10.

5. Sensitivity analysis of BMX1EF

It is important to understand how different factors affect this vibration behaviour. In this section, we perform a sensitivity analysis of the BMX1EF vibration in this particular wind turbine to investigate how the stiffness of the yaw system and different wind conditions affect this vibration. The results of this analysis can provide valuable insight into the design of the wind turbine and wind farms.

5.1. Sensitivity analysis of BMX1EF to yaw system flexibility

This sensitivity study analyses how the amplitude of BMX1EF changes when the stiffness of the yaw system is varied. To do this, the load case used in this study is the one with the highest BMX1EF of all the normal power production load cases (DLC1.2) of IEC61400-1 ed4 [49].

Fig. 11 shows part of the M_x time series data obtained in the aeroelastic simulations for different yaw stiffness values, in which different 4P contents are observed. The red colour gradient is used to highlight the series with the highest 4P content (the more red, the more 4P content). It can be seen that the lower the yaw spring stiffness, the higher the 4P content. The yaw spring stiffness is given as a multiple of the reference stiffness (k_{ref}), which is the value that best validates the simulations against the field measurements.

Fig. 12 shows the maximum normalised value of BMX1EF obtained in each simulation. It can be seen that increasing the stiffness of the yaw system reduces the BMX1EF to a base level determined by the stiffness of the tower and nacelle components. This information can be used to improve the design of the yaw system in relation to this resonance phenomenon.

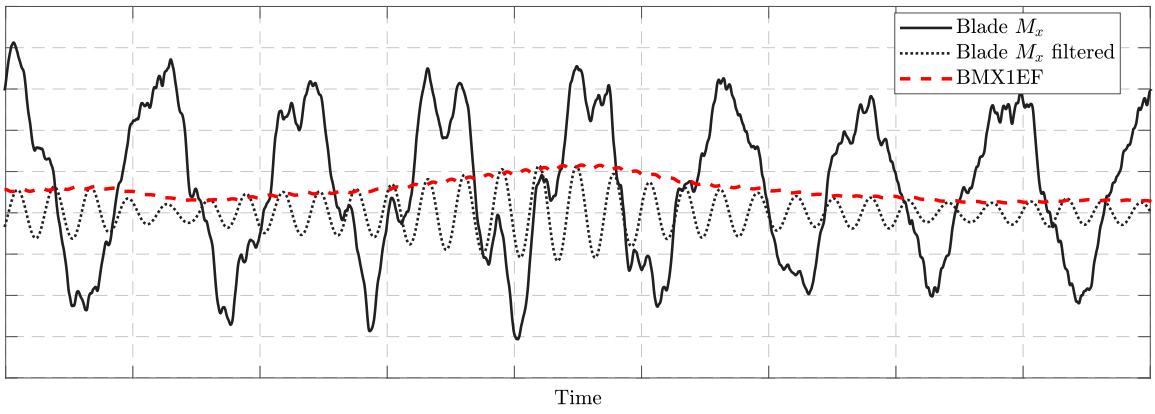

Fig. 9. Example of the filtering of the BMX1EF signal, showing the initial M_x load and the intermediate M_x filtered signal.

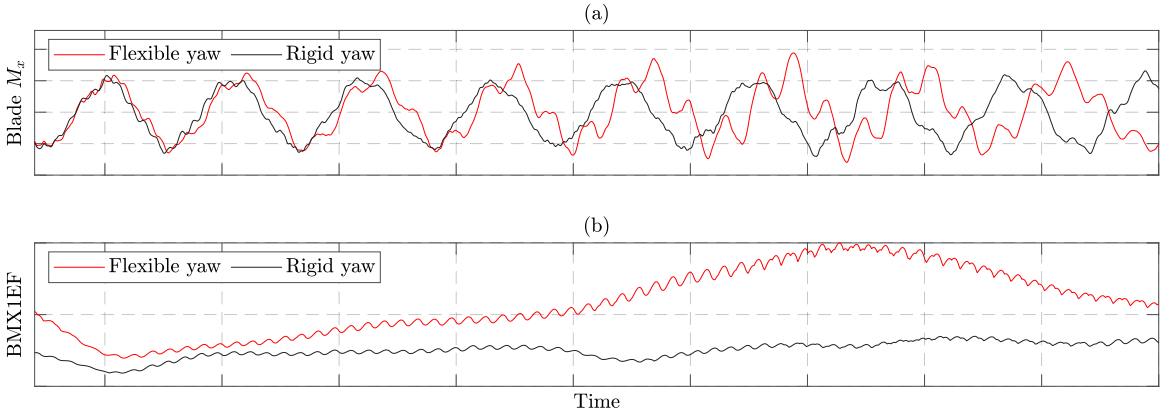

Fig. 10. Validation of proposed aeroelastic model: (a) normalised M_x, (b) normalised BMX1EF.

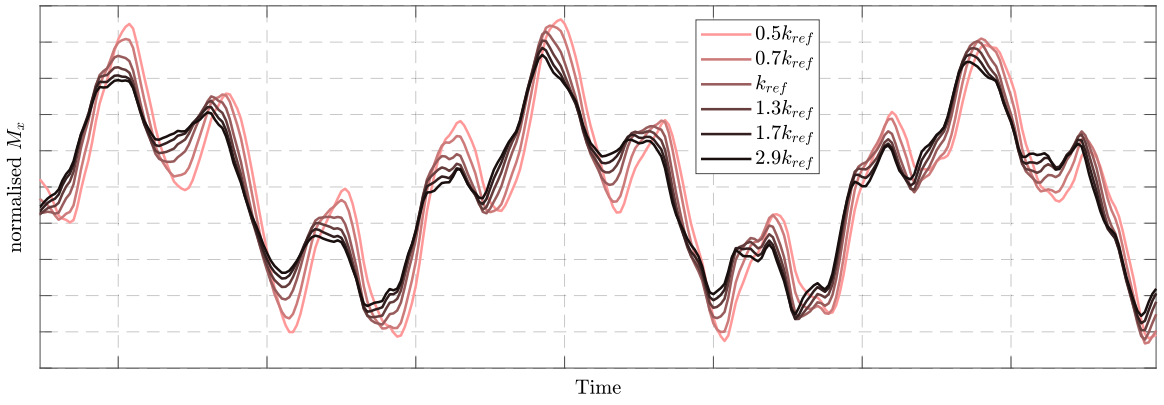

Fig. 11. Time series of normalised M_x with differences in yaw spring stiffness expressed as a multiple of the k_{ref}.

5.2. Sensitivity analysis of BMX1EF to wind conditions

This sensitivity study analyses how the vibration of the BMX1EF changes when the wind conditions that generate the fixed frame 3P loads vary. As mentioned in Section 1, these 3P loads are mainly induced by wind turbulence, wind shear, wind direction, flow inclination angle and tower shadow.

The sensitivity of the BMX1EF to some of the above wind conditions is illustrated in Fig. 13. The analysis focused specifically on the above mentioned load case, considering the k_{ref} yaw stiffness. Wind characteristics such as wind shear, tower shadow, wind direction and flow inclination angle were considered. The objective of the analysis is to assess the vulnerability of the blade edgewise vibration to fixed frame 3P loads at nominal rotor speed. Note that the ranges considered in the abcisas are the usual values for normal power production load cases.

As can be seen, the shadow of the tower (inlet-a) and the flow inclination angle (inlet-b) have a small effect on the BMX1EF vibration of about 5% between the values considered. On the other hand, wind shear (inlet-c) and wind direction (inlet-d) have a larger effect of about 20% between the values considered. The results show a low sensitivity to tower shadow and flow inclination angle, and a medium sensitivity to wind shear and wind direction.

In addition, to investigate the effect of wind turbulence on the sensitivity of the BMX1EF, some DLC1.2 scenarios are calculated using representative turbulence quantiles. These quantiles are specific statistical points within the turbulence data distribution, chosen to capture

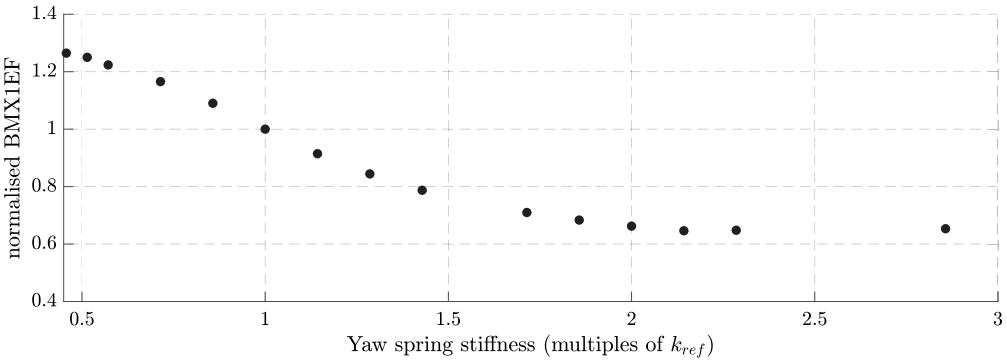

Fig. 12. Normalised BMX1EF as a function of yaw spring stiffness expressed as a multiple of the k_{ref}.

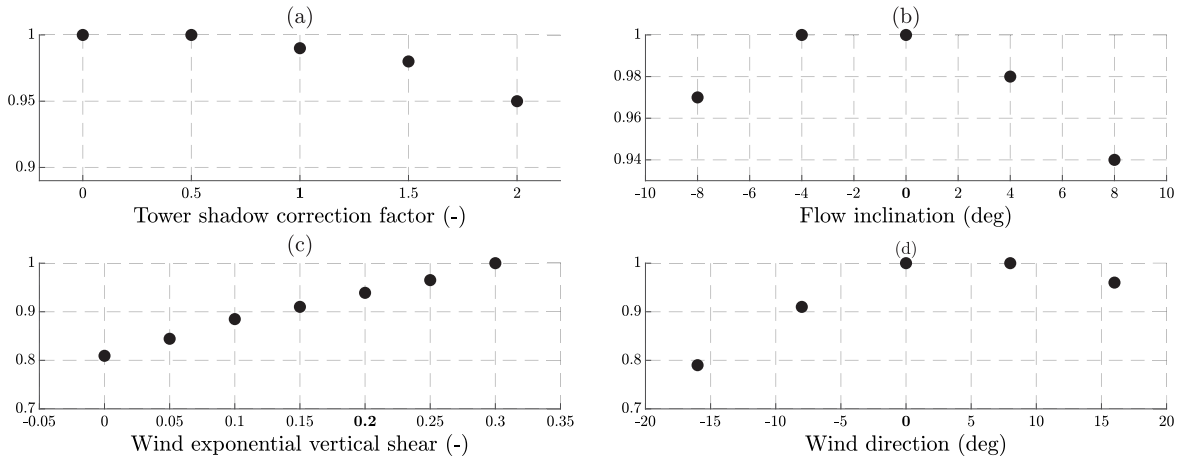

Fig. 13. Normalised BMX1EF (y-axis) as a function of wind conditions: (a) tower shadow correction factor, (b) flow inclination angle, (c) wind shear exponent, (d) wind direction. Standard values are shown in bold. Note that the scale of the normalised BMX1EF (vertical axis) is not the same in each sub-figure.

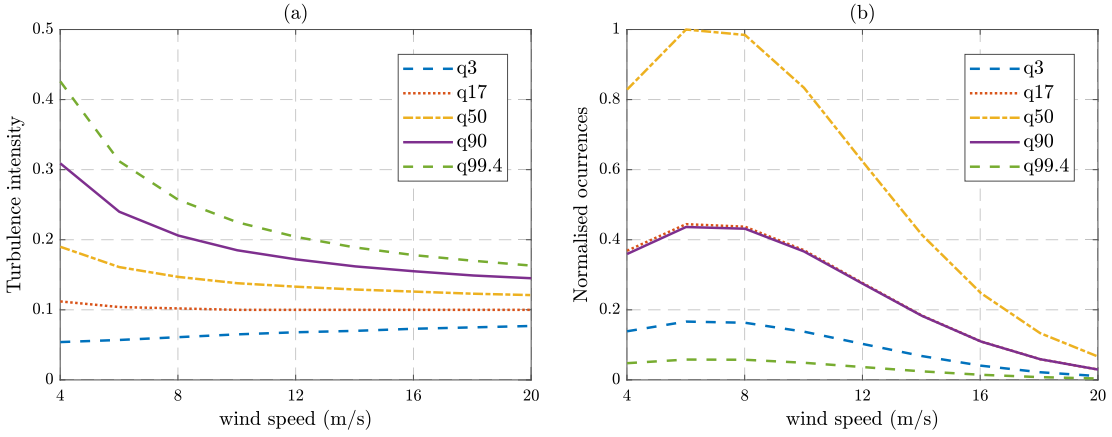

Fig. 14. Considered quantiles of the Class B turbulence distribution: (a) turbulence intensity values, (b) normalised occurrences of wind distribution.

its key characteristics [49]. The wind turbulence conditions considered in this analysis are shown in Fig. 14. The turbulence intensity values are shown in inlet-a of Fig. 14 and the normalised occurrences of the wind distribution are shown in inlet-b of Fig. 14.

Fig. 15 shows the normalised BMX1EF over different wind speeds for different turbulence levels, based on the category B turbulence standard of [49]. The figure clearly shows that both wind speed and turbulence intensity have a significant effect on the BMX1EF. The strongest vibrations are observed at high wind speeds combined with high turbulence levels.

The figure shows clear patterns in the BMX1EF under different wind conditions. On the one hand, increasing the turbulence intensity from a low quantile of 3 to a high quantile of 99.4, while keeping the wind speed constant, causes the BMX1EF value to more than double. On the other hand, increasing the wind speed from 4 m/s to 20 m/s results in at least a fourfold increase in the BMX1EF value. These observations suggest that both turbulence intensity and wind speed have a significant effect on the BMX1EF.

The figure also shows how quickly these vibrations can increase. At the higher turbulence levels, the increase in vibration is much steeper,

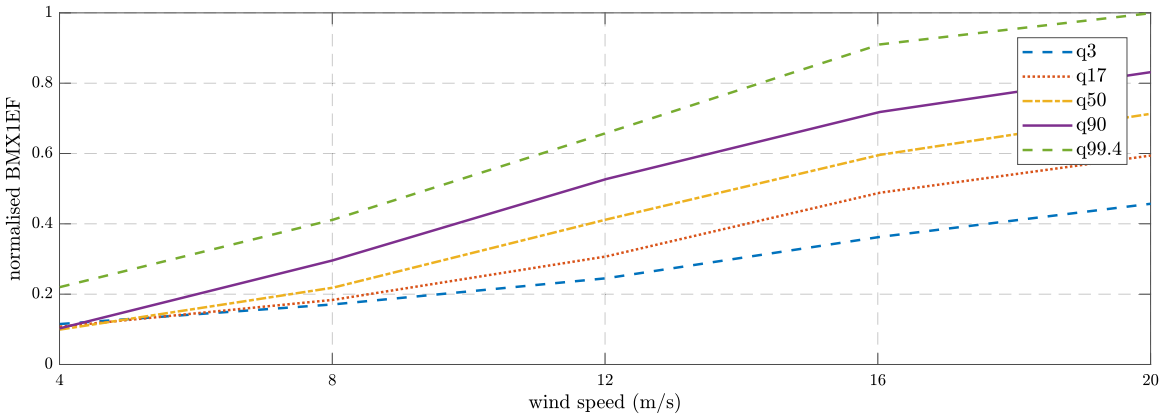

Fig. 15. Normalised BMX1EF of several turbulence quantiles of category B as a function of wind speed.

especially at wind speeds above 12 m/s. This sharp increase suggests that the effects of turbulence become more intense as the turbine faces higher wind speeds. However, it is important to put these data into perspective. Although the figure shows high BMX1EF values at high wind speeds and turbulence levels, the likelihood of both conditions occurring at the same time is quite low, especially for this class of turbine as can be seen in inlet-b of Fig. 14. This means that the impact on the BMX1EF under these conditions can be quite significant but the probability of such scenarios occurring is low.

6. Conclusions

This study provides a comprehensive investigation on mechanical loads that affect the performance and lifetime of wind turbines, with particular focus on an observed blade vibration at the 4P operational harmonic frequency that did not appear in previous aeroelastic simulations.

In this specific case, the investigation identifies that the resonance of the blade first edgewise mode at the 4P frequency results from the excitation of rotor edgewise backward whirling mode with the 3P operational harmonic.

This unexpected and unknown blade vibration has been simulated using advanced aeroelastic models that allow the effects of active yaw systems on this vibration to be included. These modelling changes made it possible to reproduce the observed field vibrations in the simulations. This improvement in the model allows better controller solutions to be designed based on the simulation data. This highlights the importance of accurate modelling to reproduce the resonance phenomenon, allowing a thorough analysis of the factors influencing it. A particularly novel finding is that by stiffening the active yaw system in this turbine, the 3P excitation on the fixed frame axes is significantly reduced, resulting in a reduction of the blade vibration at the 4P frequency.

The study also analyses the sensitivity of the observed vibration to various wind characteristics, such as wind shear, flow inclination angle, tower shadow, misalignment, turbulence intensity and wind speed. With regard to the sensitivity of the 4P vibration to the wind conditions considered, the simulations carried out show a low sensitivity to tower shadow and flow inclination angle, a medium sensitivity to wind shear and wind direction, and a particularly high sensitivity to turbulence intensity and wind speed.

In summary, this study contributes to the existing body of knowledge on wind turbine dynamics and provides a basis for future research, particularly in the modelling of active yaw systems to reproduce their dynamics during mechanical resonance phenomena.

CRediT authorship contribution statement

Antonio Torres: Conceptualization, Data curation, Formal analysis, Investigation, Methodology, Validation, Visualization, Writing – original draft, Writing – review & editing. **Javier Gil:** Conceptualization, Investigation, Methodology, Supervision, Visualization, Writing – review & editing. **Aitor Plaza:** Conceptualization, Investigation, Methodology, Supervision, Visualization, Writing – review & editing. **Jokin Aginaga:** Conceptualization, Investigation, Methodology, Supervision, Visualization, Writing – review & editing.

Declaration of competing interest

The authors declare that they have no known competing financial interests or personal relationships that could have appeared to influence the work reported in this paper.

Acknowledgements

The authors would like to thank the company Nordex for their valuable contribution to this project and acknowledge the open access funding provided by the Universidad Pública de Navarra.

References

[1] C. Anderson, Wind Turbines: Theory and Practice, 2020, http://dx.doi.org/10.1017/9781108478328.

[2] T. Burton, N. Jenkins, D. Sharpe, E. Bossanyi, Wind Energy Handbook, Wiley, 2011, URL: https://books.google.de/books?id=qVjtDxyN-joC.

[3] J. Manwell, J. Mcgowan, A. Rogers, Wind Energy Explained: Theory, Design and Application, 2009, http://dx.doi.org/10.1002/9781119994367.

[4] Y. Du, S. Zhou, X. Jing, Y. Peng, H. Wu, N. Kwok, Damage detection techniques for wind turbine blades: A review, Mech. Syst. Signal Process. 141 (2020) 106445, http://dx.doi.org/10.1016/j.ymssp.2019.106445, URL: https://www.sciencedirect.com/science/article/pii/S0888327019306661.

[5] M. Ozbek, F. Meng, D.J. Rixen, Challenges in testing and monitoring the in-operation vibration characteristics of wind turbines, Mech. Syst. Signal Process. 41 (1) (2013) 649–666, http://dx.doi.org/10.1016/j.ymssp.2013.07.023, URL: https://www.sciencedirect.com/science/article/pii/S0888327013003774.

[6] W. Weijtjens, T. Verbelen, E. Capello, C. Devriendt, Vibration based structural health monitoring of the substructures of five offshore wind turbines, Procedia Eng. 199 (2017) 2294–2299, http://dx.doi.org/10.1016/j.proeng.2017.09.187, URL: https://www.sciencedirect.com/science/article/pii/S1877705817336305. X International Conference on Structural Dynamics, EURODYN 2017.

[7] G.W.E. Council, GWEC Global Wind Report 2022, Global Wind Energy Council, Bonn, Germany, 2022.

[8] M. Abdulrahman, D. Wood, Investigating the power-COE trade-off for wind farm layout optimization considering commercial turbine selection and hub height variation, Renew. Energy 102 (2017) 267–278, http://dx.doi.org/10.1016/j.renene.2016.10.038, URL: https://www.sciencedirect.com/science/article/pii/S096014811630903X.

[9] H. Coral-Enriquez, J. Cortés-Romero, S.A. Dorado-Rojas, Rejection of varying-frequency periodic load disturbances in wind-turbines through active disturbance rejection-based control, Renew. Energy 141 (2019) 217–235, http://dx.doi.org/10.1016/j.renene.2019.04.001, URL: https://www.sciencedirect.com/science/article/pii/S0960148119304744.

[10] I. Houtzager, J.W. Wingerden, M. Verhaegen, Wind turbine load reduction by rejecting the periodic load disturbances, Wind Energy 16 (2013) 235–256, http://dx.doi.org/10.1002/we.547.

[11] S. Navalkar, J. van Wingerden, E. van Solingen, T. Oomen, E. Pasterkamp, G. van Kuik, Subspace predictive repetitive control to mitigate periodic loads on large scale wind turbines, Mechatronics 24 (8) (2014) 916–925, http://dx.doi.org/10.1016/j.mechatronics.2014.01.005, URL: https://www.sciencedirect.com/science/article/pii/S0957415814000063.

[12] A. Quilligan, A. O'Connor, V. Pakrashi, Fragility analysis of steel and concrete wind turbine towers, Eng. Struct. 36 (2012) 270–282, http://dx.doi.org/10.1016/j.engstruct.2011.12.013, URL: https://www.sciencedirect.com/science/article/pii/S0141029611004950.

[13] I.E. Commission, Wind Energy Generation Systems—Part 13: Measure of Mechanical Loads, IEC Standard 61400-13, International Electrotechnical Commission, Geneva, Switzerland, 2015.

[14] Z. Mingqiu, H. Yutong, H. Xiangsheng, J. Peng, Interpretation of wind turbine load measurement standard IEC 61400-13, in: 2019 4th International Conference on Power and Renewable Energy, ICPRE, 2019, pp. 92–95, http://dx.doi.org/10.1109/ICPRE48497.2019.9034717.

[15] C. Tibaldi, T. Kim, T.J. Larsen, F. Rasmussen, R.d. Rocca Serra, F. Sanz, An investigation on wind turbine resonant vibrations, Wind Energy 19 (5) (2016) 847–859, http://dx.doi.org/10.1002/we.1869, URL: https://onlinelibrary.wiley.com/doi/abs/10.1002/we.1869.

[16] T.L. Sullivan, A review of resonance response in large, horizontal-axis wind turbines, Sol. Energy 29 (5) (1982) 377–383, http://dx.doi.org/10.1016/0038-092X(82)90073-1, URL: https://www.sciencedirect.com/science/article/pii/0038092X82900731.

[17] P. Fleming, A. Wright, L. Fingersh, J.-W. van Wingerden, Resonant vibrations resulting from the re-engineering of a constant-speed 2-bladed turbine to a variable-speed 3-bladed turbine, in: 49th AIAA Aerospace Sciences Meeting Including the New Horizons Forum and Aerospace Exposition, http://dx.doi.org/10.2514/6.2011-634, arXiv:https://arc.aiaa.org/doi/pdf/10.2514/6.2011-634. URL: https://arc.aiaa.org/doi/abs/10.2514/6.2011-634.

[18] K. Maalawi, Special issues on design optimization of wind turbine structures, in: I. Al-Bahadly (Ed.), Wind Turbines, IntechOpen, Rijeka, 2011, http://dx.doi.org/10.5772/14716.

[19] O. Hach, H. Verdonck, J.D. Polman, C. Balzani, S. Müller, J. Rieke, H. Hennings, Wind turbine stability: Comparison of state-of-the-art aeroelastic simulation tools, J. Phys. Conf. Ser. 1618 (5) (2020) 052048, http://dx.doi.org/10.1088/1742-6596/1618/5/052048.

[20] J. Holierhoek, 5 - aeroelastic design of wind turbine blades, in: P. Brøndsted, R. Nijssen, S. Goutianos (Eds.), Advances in Wind Turbine Blade Design and Materials (Second Edition), second ed., in: Woodhead Publishing Series in Energy, Woodhead Publishing, 2023, pp. 169–189, http://dx.doi.org/10.1016/B978-0-08-103007-3.00010-0, URL: https://www.sciencedirect.com/science/article/pii/B9780081030073000100.

[21] O. Gözcü, D.R. Verelst, The effects of blade structural model fidelity on wind turbine load analysis and computation time, Wind Energy Sci. 5 (2) (2020) 503–517, http://dx.doi.org/10.5194/wes-5-503-2020, URL: https://wes.copernicus.org/articles/5/503/2020/.

[22] M. Sayed, L. Klein, T. Lutz, E. Krämer, The impact of the aerodynamic model fidelity on the aeroelastic response of a multi-megawatt wind turbine, Renew. Energy 140 (2019) 304–318, http://dx.doi.org/10.1016/j.renene.2019.03.046, URL: https://www.sciencedirect.com/science/article/pii/S0960148119303519.

[23] O.T. Filsoof, X. Zhang, An intuitive representation and analysis of multi-rotor wind turbine whirling modes, Wind Energy 25 (3) (2022) 553–572, http://dx.doi.org/10.1002/we.2686, URL: https://onlinelibrary.wiley.com/doi/abs/10.1002/we.2686.

[24] O.T. Filsoof, M.H. Hansen, A. Yde, P.B. ttcher, X. Zhang, A novel methodology for analyzing modal dynamics of multi-rotor wind turbines, J. Sound Vib. 493 (2021) 115810, http://dx.doi.org/10.1016/j.jsv.2020.115810, URL: https://www.sciencedirect.com/science/article/pii/S0022460X20306398.

[25] G. Wanke, L. Bergami, D.R. Verelst, Differences in damping of edgewise whirl modes operating an upwind turbine in a downwind configuration, Wind Energy Sci. 5 (3) (2020) 929–944, http://dx.doi.org/10.5194/wes-5-929-2020, URL: https://wes.copernicus.org/articles/5/929/2020/.

[26] Y. Zhao, J. Pan, Z. Huang, Y. Miao, J. Jiang, Z. Wang, Analysis of vibration monitoring data of an onshore wind turbine under different operational conditions, Eng. Struct. 205 (2020) 110071, http://dx.doi.org/10.1016/j.engstruct.2019.110071, URL: https://www.sciencedirect.com/science/article/pii/S0141029619302044.

[27] D. Tcherniak, J. Basurko, O. Salgado, I. Urresti, S. Chauhan, C.E. Carcangiu, M. Rossetti, Application of OMA to operational wind turbine, in: Proceedings of 4th International Operational Modal Analysis Conference, 2011.

[28] G. Bir, Multi-blade coordinate transformation and its application to wind turbine analysis, in: 46th AIAA Aerospace Sciences Meeting and Exhibit, 2008, p. 1300.

[29] M. Hansen, Improved modal dynamics of wind turbines to avoid stall-induced vibrations, Wind Energy 6 (2003) 179–195, http://dx.doi.org/10.1002/we.79.

[30] J. Thirstrup Petersen, K. Thomsen, H. Aagaard Madsen, Local Blade Whirl and Global Rotor Whirl Interaction, in: Denmark. Forskningscenter Risoe. Risoe-R, number 1067(EN), 1998.

[31] Z. Zhang, S.R.K. Nielsen, F. Blaabjerg, D. Zhou, Dynamics and control of lateral tower vibrations in offshore wind turbines by means of active generator torque, Energies 7 (11) (2014) 7746–7772, http://dx.doi.org/10.3390/en7117746, URL: https://www.mdpi.com/1996-1073/7/11/7746.

[32] G. Mandic, A. Nasiri, E. Muljadi, F. Oyague, Active torque control for gearbox load reduction in a variable-speed wind turbine, IEEE Trans. Ind. Appl. 48 (6) (2012) 2424–2432, http://dx.doi.org/10.1109/TIA.2012.2227131.

[33] J. Licari, C.E. Ugalde-Loo, J.B. Ekanayake, N. Jenkins, Damping of torsional vibrations in a variable-speed wind turbine, IEEE Trans. Energy Convers. 28 (1) (2013) 172–180, http://dx.doi.org/10.1109/TEC.2012.2224868.

[34] S. Oh, Statistical study of the effect of wind characteristics on the main shaft loadings of an active-stall controlled wind turbine, J. Phys. Conf. Ser. 753 (2016) http://dx.doi.org/10.1088/1742-6596/753/11/112012.

[35] Bladed, Bladed (Version 4.13) [computer software], 2023, URL: https://www.dnvgl.com/software/bladed.html. Retrieved March 16, 2023.

[36] DNV, Bladed User Manual: Version 4.13, vol. 550, DNV Services UK Limited 2022, 2022.

[37] DNV, Bladed Theory Manual: Version 4.13, vol. 550, DNV Services UK Limited 2022, 2022.

[38] J.M.R. Bampton, Coupling of substructures for dynamic analyses, AIAA J. 6 (1968) 1313–1319, http://dx.doi.org/10.2514/3.4741.

[39] J. Craig, Coupling of substructures for dynamic analyses - an overview, in: 41st Structures, Structural Dynamics, and Materials Conference and Exhibit, 2000, http://dx.doi.org/10.2514/6.2000-1573.

[40] H. Glauert, A General Theory of the Autogyro, Technical Report, 1111, ARC R&M, 1926.

[41] S. Øye, Tjæreborg wind turbine: 4. dynamic inflow measurement, 1991.

[42] S. Øye, Induced velocities for rotors in yaw, in: Proceedings of the Sixth IEA Symposium, Energy Research Centre of the Netherlands Petten, 1992, pp. 1–5.

[43] H. Snel, J. Schepers, Joint investigation of dynamic inflow effects and implementation of an engineering method, 1995.

[44] M. Hansen, M. Gaunaa, H. Madsen, A Beddoes–Leishman type dynamic stall model in state-space and indicial formulations, 2004.

[45] E. Menezes, A. Araújo, N. Bouchonneau, A review on wind turbine control and its associated methods, J. Clean. Prod. 174 (2017) http://dx.doi.org/10.1016/j.jclepro.2017.10.297.

[46] J.G. Njiri, D. Söffker, State-of-the-art in wind turbine control: Trends and challenges, Renew. Sustain. Energy Rev. 60 (2016) http://dx.doi.org/10.1016/j.rser.2016.01.110.

[47] R. Gao, Z. Gao, Pitch control for wind turbine systems using optimization, estimation and compensation, Renew. Energy 91 (2016) 501–515, http://dx.doi.org/10.1016/j.renene.2016.01.057.

[48] V. Petrović, M. Jelavić, M. Baotić, Advanced control algorithms for reduction of wind turbine structural loads, Renew. Energy 76 (2015) 418–431, http://dx.doi.org/10.1016/j.renene.2014.11.051.

[49] International Electrotechnical Commission, Wind Energy Generation Systems—Part 1: Design Requirements, fourth ed., International Electrotechnical Commission, Geneva, Switzerland, 2019.